Supporting Material

Retinal Flip in Rhodopsin Activation?

Jun Feng,[1] Michael F. Brown,[2,3] and Blake Mertz[1]

[1]The C. Eugene Bennett Department of Chemistry, West Virginia University, Morgantown, West Virginia, USA. [2]Department of Chemistry and Biochemistry, University of Arizona, Tucson, Arizona, USA. [3]Department of Physics, University of Arizona, Tucson, Arizona, USA.

Contents:

Computational Methods

The initial structure of rhodopsin for the simulation was taken from the Meta-II state (PDB 3PXO). Crystal waters were retained for the simulation setup and no extra water molecules were added in the interior of protein. The principal axis of the protein was oriented parallel to the *z*-axis with the center of mass moved to the origin. To favor the reversible Meta-II to Meta-I back transition, the protonation states of amino acid residues were assigned according to the inactive Meta-I state. Specifically, residues Asp83$^{2.54}$ and Glu122$^{3.37}$ were protonated, and all other ionizable residues carried their standard charges at physiological pH (1). The all-*trans* ligand retinal was bound to Lys296$^{6.43}$ via a protonated Schiff base (15-*anti*). Both Glu113$^{3.28}$ and Glu181^{EL2} were deprotonated to reflect a complex counterion in the binding pocket, which has been verified experimentally by FTIR and solid-state ^{2}H NMR spectroscopy, and with MD simulations (2,3). In addition, Glu134$^{3.49}$, which undergoes cytoplasmic proton uptake only in the fully active Meta-II state, was deprotonated. To simulate the Meta-II state, Asp83$^{2.54}$, Glu113$^{3.28}$, and Glu122$^{3.37}$ were protonated, but the Schiff base was deprotonated. In all simulations, two palmitate molecules were covalently linked to Cys322^{CT} and Cys323^{CT}, respectively, with the aliphatic chains approximately parallel to the *z*-axis.

The replacement method of the Membrane Builder (4,5) from the CHARMM-GUI website (http://www.charmm-gui.org) was used to set up rhodopsin in an explicit hydrated lipid bilayer. To study the Meta-II to Meta-I state transition, three simulation systems were set up with different lipid bilayer compositions, i.e., DOPC/DOPE ratios of 3:1, 1:1, and 1:3, with 128 lipids in each leaflet (**Table S3**). One control simulation system was set up to favor the Meta-II state with a DOPC/DOPE ratio of 1:3. The protein and lipid bilayer were hydrated with at least 3 layers (~10 Å) of TIP3P water. Sodium and chloride ions were added to the simulation box to neutralize the system and maintain a salt concentration of 0.15 M. The final dimension of each system was approximately 100 Å × 100 Å × 95 Å.

All simulations were set up using CHARMM (6) and the MMTSB toolset (7) with the c36 CHARMM force field (8,9). The force field parameters of retinal were from Feller and coworkers (10,11). The simulations were initially run in NAMD (12) and then transferred using CHAMBER (13) to run in

AMBER12 (14) utilizing graphics processing unit (GPU) acceleration. All simulations were performed in the *NPT* ensemble. Langevin dynamics were used for temperature control at 300 K with a collision frequency of 5 ps^{-1}. Berendsen (15) non-isotropic pressure scaling with a relaxation time of 8 ps was employed for the membrane simulations. A timestep of 2 fs was used with bonds constrained with the SHAKE algorithm. Each trajectory was 3 μs long for a total of 12 μs simulation time. Coordinates were saved every 10 ps. Analysis was carried out using CHARMM (6), MDAnalysis (16), LOOS (17), and in-house scripts. Molecular visualization was done in VMD (18) and PyMOL (19).

Supplementary Table S1. Principal component analysis of retinal and rhodopsin in MD simulations.

Simulation	DOPC:DOPE	rhodopsin[a]			retinal		
		PC1[b]	PC2	PC3	PC1	PC2	PC3
Meta-II to Meta-I transition	3:1	36.12	11.78	6.48	75.76	6.03	4.67
	1:1	41.88	12.50	6.58	67.72	13.36	4.94
	1:3	27.00	10.56	8.20	64.09	14.03	4.71
Meta-II control	1:3	47.75	6.80	5.94	33.55	18.10	13.40

[a] Proportion (in percentage) of structural fluctuations captured by first, second, and third principal components (PC1, PC2, and PC3) in each simulation.

[b] Principal component analysis was applied to the C_α atoms of seven transmembrane helices (rhodopsin) and heavy atoms of retinal (retinal), respectively.

Supplementary Table S2. Correlation between first principal components of rhodopsin and retinal.

Simulation	lipid:lipid	$r_{\mathrm{RHO,RET}}$[a]
DOPC:DOPE	3:1	-0.76
DOPC:DOPE	1:1	0.70
DOPC:DOPE	1:3	-0.52
Meta-II	1:3	0.58

[a] The correlation between any other PC is negligible ($|r| \ll 0.3$).

Supplementary Table S3. Proteolipid systems modeled and details of each simulation.

simulation[a]	DOPC:DOPE[b]	lipid:protein[c]	# of atoms	retinal flip[b]	Glu113$^{3.28d}$	Glu134$^{3.49e}$	Schiff base[f]
Meta-II to Meta-I transition	3:1	256:1	94,789	yes	–	–	+
	1:1	256:1	94,405	no	–	–	+
	1:3	256:1	93,913	yes	–	–	+
Meta-II control	1:3	256:1	93,871	no	neutral	neutral	neutral

[a] All simulations started from Meta-II configuration (PDB ID 3PXO).
[b] Molar ratio.
[c] Yes = polyene chain underwent reorientation of the methyl groups towards the extracellular lid of rhodopsin.
[d] Counterion to the Schiff base and accepts proton from protonated Schiff base in the Meta-II state.
[e] Part of the conserved "ionic lock" in Class A GPCRs that undergoes proton uptake in Meta-II state.
[f] Covalent linkage between the retinal chromophore and the sidechain of Lys296$^{6.43}$, protonated until Meta-II state.

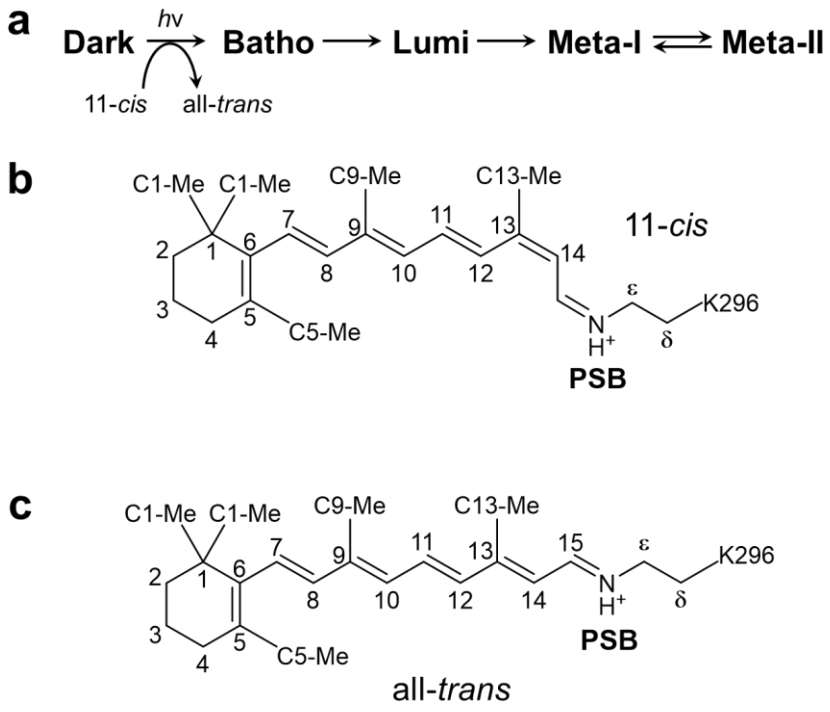

Supplementary Figure S1. Photocascade of rhodopsin is directly tied to action of the retinal chromophore. (a) The photocascade of rhodopsin. In the dark state, retinal is in the 11-*cis* conformation. Upon absorption of a photon, the retinal undergoes a *cis* to *trans* isomerization, facilitating the progression of rhodopsin through a series of photointermediates until it reaches equilibrium between the inactive Meta-I and active Meta-II states. 11-*cis* (b) and all-*trans* (c) forms of retinal. Note the protonated Schiff base (PSB) linkage to the side chain of Lys296$^{6.43}$.

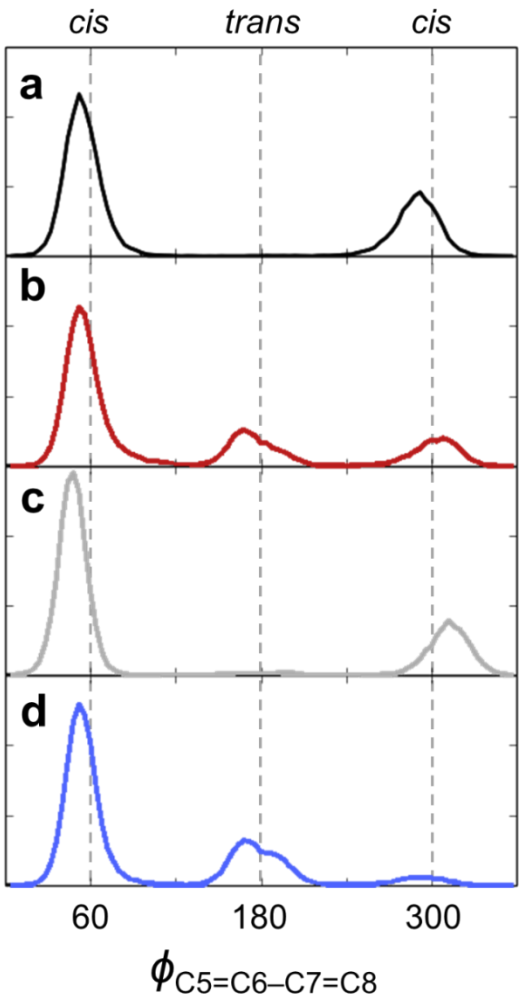

Supplementary Figure S2. The β-ionone ring of retinal can adopt both *cis* and *trans* conformations in the Meta-II state. Normalized distribution of the C5=C6–C7=C8 dihedral angle between the β-ionone ring and the polyene chain of retinal. When the retinal polyene chain methyl groups are oriented towards the cytoplasmic side of the protein, the β-ionone ring fluctuates between 6-*s*-*cis* conformations (60 and 300 deg, respectively). However, after a flip of the polyene chain and orientation toward the extracellular lid, the β-ionone ring adopts a 6-*s*-*trans* conformation (180 deg). (a) Rhodopsin in the Meta-II protonation states embedded in a DOPC:DOPE (3:1 molar ratio) bilayer, (b) rhodopsin in the Meta-I protonation states embedded in a DOPC:DOPE (1:3) bilayer, (c) rhodopsin (Meta-I) in a DOPC:DOPE (1:1) bilayer, and (d) rhodopsin (Meta-I) in a DOPC:DOPE (3:1) bilayer.

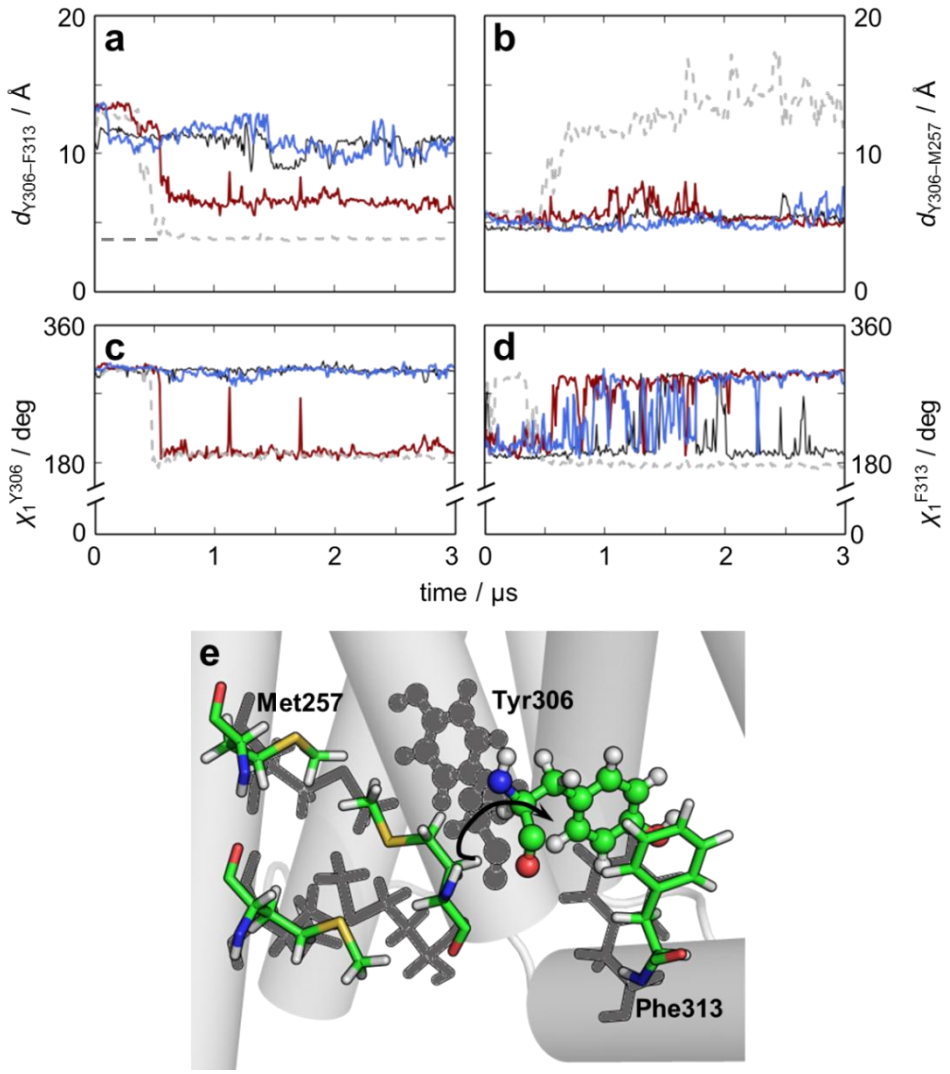

Supplementary Figure S3. The NPxxY motif fluctuates between active and inactive conformations during molecular (MD) simulations. (a) Stabilizing aromatic stacking interactions are reestablished between Tyr306$^{7.53}$ and Phe313$^{7.60}$ in two of the DOPC:DOPE simulations; *black*: Meta-II; *blue*: DOPC/DOPE (3:1); *gray*: DOPC/DOPE (1:1); *red*: DOPC/DOPE (1:3). (b) Breaking of interactions between Tyr306$^{7.53}$ and Met257$^{6.40}$ is not always required. (c) Reestablishment of stacking interactions is due to rotation of Tyr306$^{7.53}$ around the χ_1 dihedral but (d) not χ_1 of Phe313$^{7.60}$. (e) Representative snapshots from MD trajectories show that the NPxxY motif has several modes of nonbonded interactions between interleaved methionine sidechains in TM6 and TM7 (gray outline: DOPC/DOPE (3:1); green: DOPC/DOPE (1:1)).

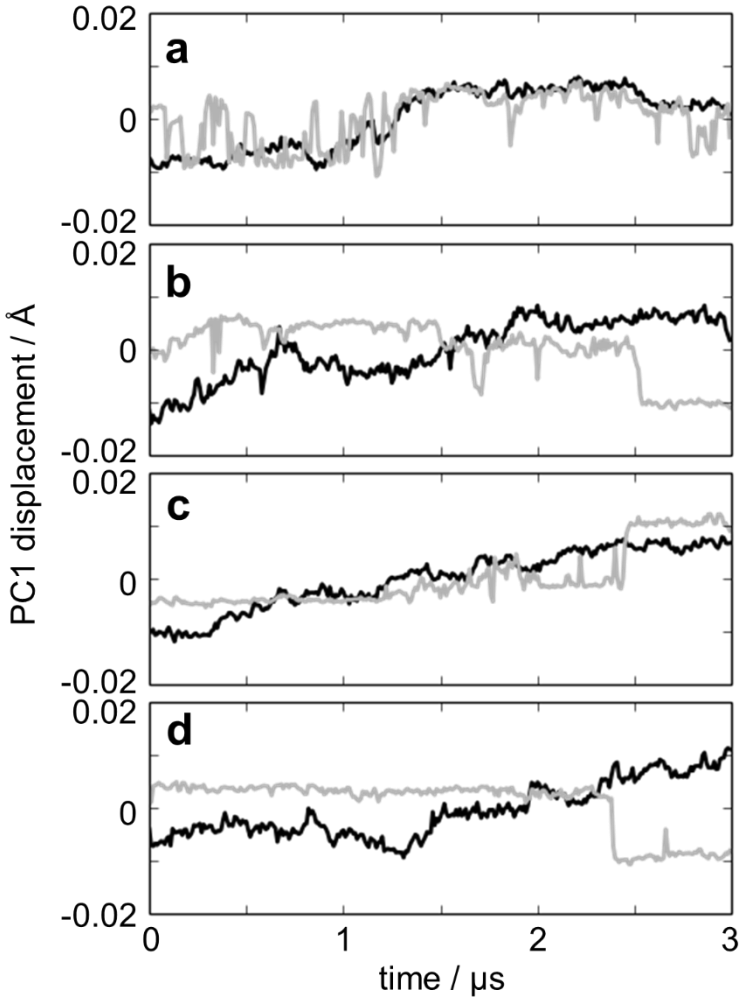

Supplementary Figure S4. Time evolution of the first principal components of retinal and rhodopsin. PC1s are shown for retinal (*gray*) and rhodopsin (*black*) over the course of the MD simulations, demonstrating loose coupling between the two components. (a) Meta-II, (b) DOPC:DOPE (1:3), (c) DOPC:DOPE (1:1), (d) DOPC:DOPE (3:1).

Supplementary discussion

After verifying the stability of our system and that it reproduces the lipid bilayer properties (**Table S4** and **Fig. S5**), we examined characteristics that are structural hallmarks for the transition of rhodopsin from the Meta-II to the Meta-I state. Rearrangements of key amino acid side chains within the retinal binding pocket that facilitate the transition to the active Meta-II state, such as Ile189^{EL2}, Tyr191^{EL2}, Trp265$^{6.47}$, and Tyr268$^{6.51}$ (20), are intimately involved with the retinal cofactor. In addition to the stabilizing interactions with the C9-methyl group, Tyr191^{EL2} also stabilizes the C13-methyl group (**Fig. S6**). However, the majority of binding pocket interactions that are notably different between crystallographic (21) and NMR (22) studies are stable, regardless of the retinal flip. These rearrangements of side chains parallel to the long axis of the polyene chain contribute to the stabilization of retinal oriented towards the extracellular lid of rhodopsin for the remainder of the simulation (~500 ns). Moreover, the region surrounding the β-ionone ring is surprisingly stable, providing an environmental context to the quantum chemical studies conducted *in vacuo* that recently identified a direct correlation between the C5=C6–C7=C8 dihedral and the pK_a of the Schiff base (10). These studies showed that the SB possessed a pK_a favorable to deprotonation (< 7) when the β-ionone ring was in a twisted 6-*s*-*cis* conformation, whereas a 6-*s*-*trans* conformation favored a protonated SB (> 9). It appears that the energy barrier is greater for rotation of the β-ionone ring rather than the polyene chain, contrary to what had been shown for rhodopsin in the dark state (23). Nevertheless, our results agree with the original hypothesis that the β-ionone ring can sample multiple conformations (*cis* or *trans*) (**Fig. S2**), which in our case is due to fluctuations of the polyene chain, rather than the ionone ring.

Another important aspect is that hydration of the protein interior changes during rhodopsin activation, although it has been difficult to characterize (24). Our MD simulations (25) as well as crystal structures (26) have identified a possible water channel that connects the cytoplasmic side of the protein with the retinal binding pocket. Together with the helical tilt of TM5 and outward rotation of TM6 in the active state (27), there is evidence for an increase in the internal protein volume that is accessible to bulk solution. By contrast, several studies have postulated that the Meta-II state is accessible only *via*

dehydration (28,29), which has led to conflicting views on the role of water flux in rhodopsin activation. Our results tend to favor the former view; it is conceivable that with longer timescales, we could potentially observe larger-scale conformational changes in the TM helical bundle that could shed more light on this critical issue.

Previous long-timescale MD simulation studies conducted on the β_2-adrenergic receptor revealed loose coupling between the movements of the agonist binding pocket, the G protein binding site, and a connector region that links the two (30). Since rhodopsin is a Class A GPRCR like the β_2-adrenergic receptor, it would be highly relevant to see if the motions of retinal acting as an agonist in the Meta-II state have a similar effect on the overall motions of the protein. We conducted principal component analysis (PCA) of the retinal chromophore and the apo form of rhodopsin in order to determine the dominant motions over the course of our simulations. Our results show that the first principal component (PC1) captures the majority of the retinal fluctuations in each of the DOPC/DOPE simulations, but not in the Meta-II simulation (**Table S1**). PC1 of the protein is less dominant in all simulations, capturing less than half of the structural fluctuations, indicating that the motions of rhodopsin are much more complex than the chromophore.

To assess the relationship between principal components (PCs) of the retinal and rhodopsin, we calculated the correlation coefficient among first ten PCs, $r\left(\mathrm{PC}_i^{\mathrm{RHO}}, \mathrm{PC}_j^{\mathrm{RET}}\right)$ for $1 \leq i, j \leq 10$. The results reveal that the motions of the retinal and rhodopsin are not strongly correlated (**Table S2**), and this can also be seen in the time evolution of PC1 for retinal and rhodopsin (**Fig. S3**). This finding appears to support the hypothesis suggested by Dror and coworkers that identified loose coupling between agonist binding and conformational changes within the G protein binding site on the cytoplasmic side of the β_2-adrenergic receptor (30). However, further investigation in our rhodopsin systems and in other GPCR systems is necessary in order to more fully understand this structural behavior.

Supplementary Table S4. Area per lipid at aqueous interface.

Simulation[a,b]	lipid:lipid[c]	Area per Lipid[c,d] / Å^2
Meta-II	3:1	61.2±0.7
1DOPC:3DOPE	1:1	61.6±0.9
1DOPC:1DOPE	1:3	62.9±0.9
3DOPC:1DOPE	1:3	64.6±0.9

[a] Calculated from trajectory after 0.5 μs.
[b] Protein cross-sectional area estimated to be 1242 Å^2.
[c] Molar ratio
[d] Values of surface area per lipid from pure DOPC system using CHARMM c36 force field at 303 K is 69.0±0.3 Å^2.[1]
[e] Experimental values of surface area per lipid are 67.4±1.0 Å^2 for DOPC at 303 K (31) and 60 Å^2 for DOPE at 271 K (32).

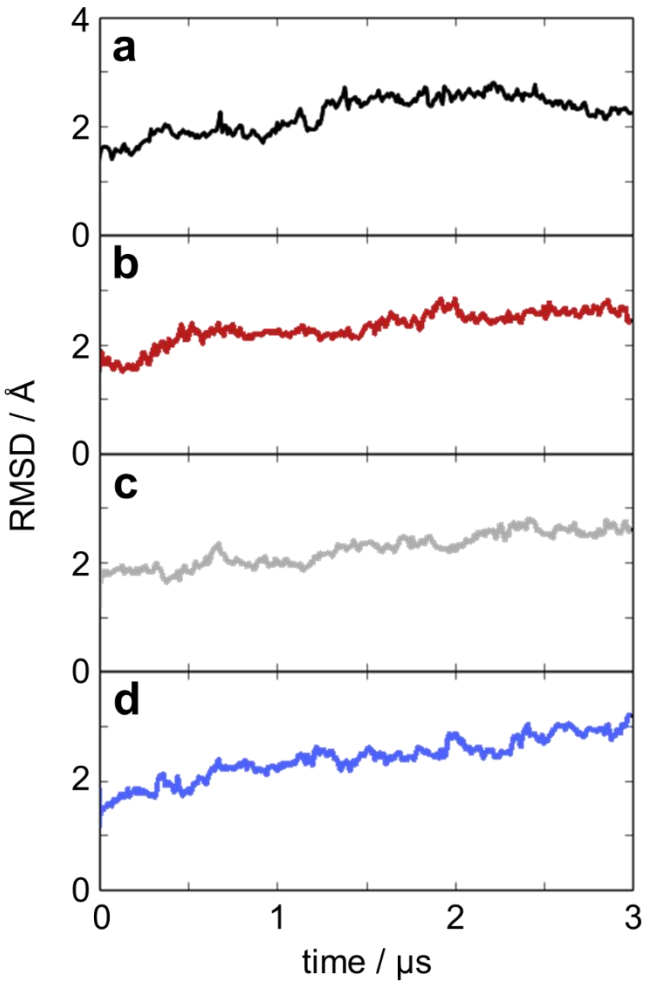

Supplementary Figure S5. Heavy-atom root-mean-square-deviation (RMSD) of seven transmembrane helices from Meta II crystal structure. RMSDs were calculated in order to verify stability of the heptahelical bundle over microsecond timescales. (a) Meta-II, (b) DOPC:DOPE (1:3), (c) DOPC:DOPE (1:1), (d) DOPC:DOPE (3:1).

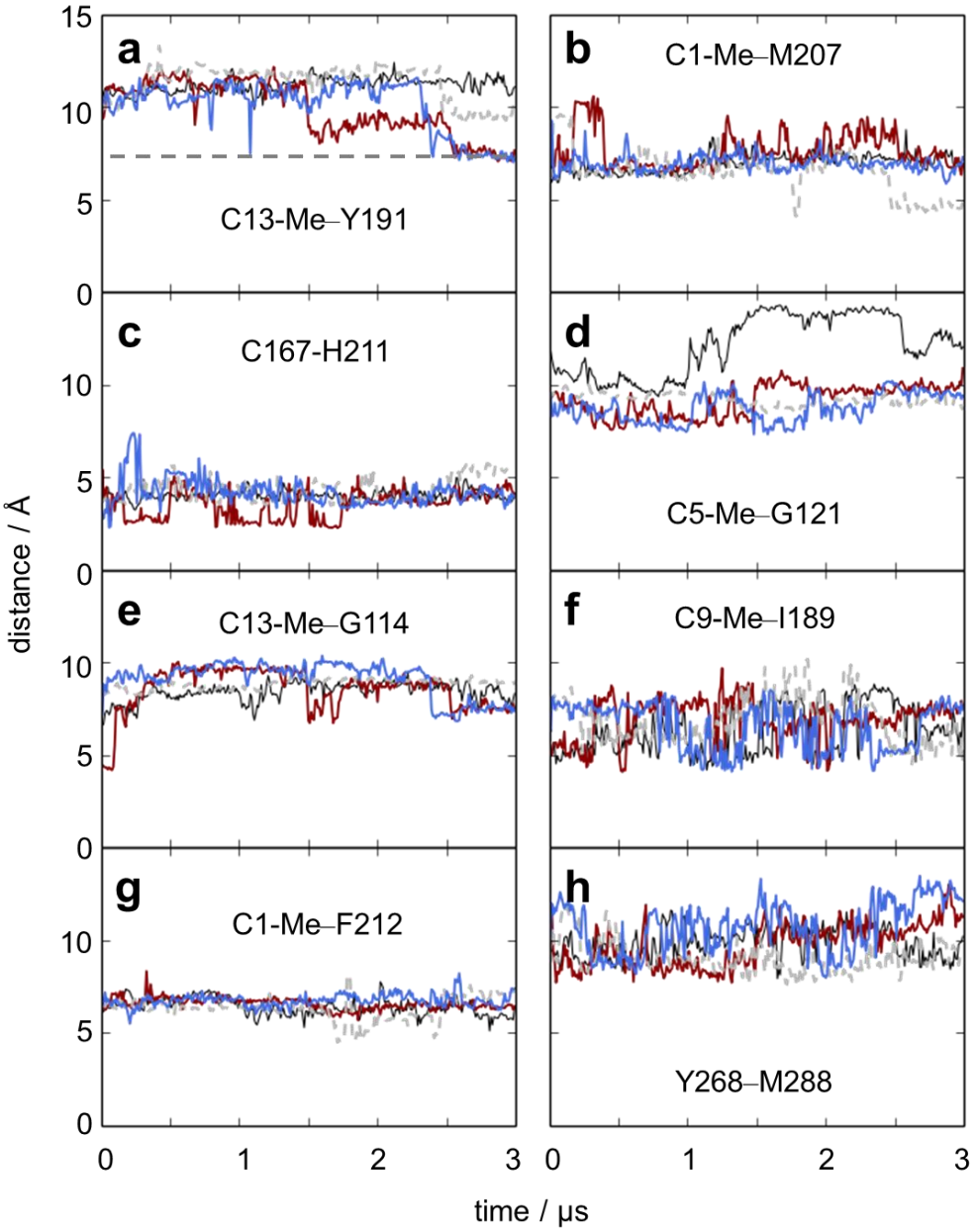

Supplementary Figure S6. Retinal binding pocket stabilizes the retinal polyene chain in two different orientations. After the retinal flip, interactions between the C13-methyl and Tyr191^{EL2} are restored (a). However, the majority of binding pocket interactions that are notably different between crystallographic (21) and NMR studies (22) are stable regardless of the retinal orientation (b-h).

Supplementary Movie S1. Flip of retinal in the binding pocket. Time evolution from the DOPC:DOPE (3:1) trajectory in which the polyene chain flips from the cytoplasmic side of the protein and Trp265$^{6.48}$ (bottom) towards the extracellular lid of the protein and Tyr191^{EL2} (top). Note the two-state conformation of the polyene chain ("down" to "up") and the fluctuation of the Trp265$^{6.48}$ χ_1 dihedral (part of the "transmission switch" (33)).

Supporting References

1. Periole, X., M.A. Ceruso, and E.L. Mehler. 2004. Acid−Base Equilibria in Rhodopsin: Dependence of the Protonation State of Glu134 on Its Environment. Biochemistry 43: 6858–6864.

2. Ludeke, S., M. Beck, E.C.Y. Yan, T.P. Sakmar, F. Siebert, and R. Vogel. 2005. The Role of Glu181 in the Photoactivation of Rhodopsin. J. Mol. Biol. 353: 345–356.

3. Martinez-Mayorga, K., M.C. Pitman, A. Grossfield, S.E. Feller, and M.F. Brown. 2006. Retinal Counterion Switch Mechanism in Vision Evaluated by Molecular Simulations. J. Am. Chem. Soc. 128: 16502–16503.

4. Jo, S., T. Kim, and W. Im. 2007. Automated Builder and Database of Protein/Membrane Complexes for Molecular Dynamics Simulations. PLoS ONE. 2: e880.

5. Jo, S., J.B. Lim, J.B. Klauda, and W. Im. 2009. CHARMM-GUI Membrane Builder for Mixed Bilayers and Its Application to Yeast Membranes. Biophys. J. 97: 50–58.

6. Brooks, B.R., C.L. Brooks, A.D. Mackerell, L. Nilsson, R.J. Petrella, B. Roux, Y. Won, G. Archontis, C. Bartels, S. Boresch, A. Caflisch, L. Caves, Q. Cui, A.R. Dinner, M. Feig, S. Fischer, J. Gao, M. Hodoscek, W. Im, K. Kuczera, T. Lazaridis, J. Ma, V. Ovchinnikov, E. Paci, R.W. Pastor, C.B. Post, J.Z. Pu, M. Schaefer, B. Tidor, R.M. Venable, H.L. Woodcock, X. Wu, W. Yang, D.M. York, and M. Karplus. 2009. CHARMM: The biomolecular simulation program. J. Comput. Chem. 30: 1545–1614.

7. Feig, M., J. Karanicolas, and C.L. Brooks III. 2004. MMTSB Tool Set: enhanced sampling and multiscale modeling methods for applications in structural biology. J. Mol. Graph. Model. 22: 377–395.

8. Klauda, J.B., V. Monje, T. Kim, and W. Im. 2012. Improving the CHARMM Force Field for Polyunsaturated Fatty Acid Chains. J. Phys. Chem. B. 116: 9424–9431.

9. Best, R.B., X. Zhu, J. Shim, P.E.M. Lopes, J. Mittal, M. Feig, and A.D. MacKerell. 2012. Optimization of the Additive CHARMM All-Atom Protein Force Field Targeting Improved Sampling of the Backbone ϕ, ψ and Side-Chain χ1 and χ2 Dihedral Angles. J. Chem. Theory Comput. 8: 3257–3273.

10. Zhu, S., M.F. Brown, and S.E. Feller. 2013. Retinal Conformation Governs pKa of Protonated Schiff Base in Rhodopsin Activation. J. Am. Chem. Soc. 135: 9391–9398.

11. Mertz, B., M. Lu, M.F. Brown, and S.E. Feller. 2011. Steric and electronic influences on the torsional energy landscape of retinal. Biophys. J. 101: L17–19.

12. Phillips, J.C., R. Braun, W. Wang, J. Gumbart, E. Tajkhorshid, E. Villa, C. Chipot, R.D. Skeel, L. Kalé, and K. Schulten. 2005. Scalable molecular dynamics with NAMD. J. Comput. Chem. 26: 1781–1802.

13. Crowley, M.F., M.J. Williamson, and R.C. Walker. 2009. CHAMBER: Comprehensive support for CHARMM force fields within the AMBER software. Int. J. Quantum Chem. 109: 3767–3772.

14. Case, D.A., T.A. Darden, T.E. Cheatham III, C.L. Simmerling, J. Wang, R.E. Duke, R. Luo, R.C. Walker, W. Zhang, K.M. Merz, B. Roberts, S. Hayik, A. Roitberg, G. Seabra, J. Swails, A.W. Goetz, I. Kolossvary, K.F. Wong, F. Paesani, J. Vanicek, R.M. Wolf, J. Liu, X. Wu, S.R. Brozell, T. Steinbrecher, H. Gohlke, Q. Cai, X. Ye, J. Wang, M.-J. Hsieh, G. Cui, D.R. Roe, D.H. Mathews, M.G. Seetin, R. Salomón-Ferrer, C. Sagui, V. Babin, T. Luchko, S. Gusarov, A. Kovalenko, and P.A. Kollman. 2012. Amber 12. University of California, San Francisco.

15. Berendsen, H.J.C., J.P.M. Postma, W.F. van Gunsteren, A. DiNola, and J.R. Haak. 1984. Molecular dynamics with coupling to an external bath. J. Chem. Phys. 81: 3684–3690.

16. Michaud-Agrawal, N., E.J. Denning, T.B. Woolf, and O. Beckstein. 2011. MDAnalysis: A toolkit for the analysis of molecular dynamics simulations. J. Comput. Chem. 32: 2319–2327.

17. Romo, T.D., N. Leioatts, and A. Grossfield. 2014. Lightweight object oriented structure analysis: Tools for building tools to analyze molecular dynamics simulations. J. Comput. Chem. 35: 2305–2318.

18. Humphrey, W., A. Dalke, and K. Schulten. 1996. VMD: visual molecular dynamics. J. Mol. Graph. 14: 33–38, 27–28.

19. The PyMOL Molecular Graphics System, Version 1.7.0. Schrödinger, LLC.

20. Vogel, R., S. Lüdeke, F. Siebert, T.P. Sakmar, A. Hirshfeld, and M. Sheves. 2006. Agonists and partial agonists of rhodopsin: retinal polyene methylation affects receptor activation. Biochemistry 45: 1640–1652.

21. Choe, H.-W., Y.J. Kim, J.H. Park, T. Morizumi, E.F. Pai, N. Krausz, K.P. Hofmann, P. Scheerer, and O.P. Ernst. 2011. Crystal structure of metarhodopsin II. Nature. 471: 651–655.

22. Ahuja, S., E. Crocker, M. Eilers, V. Hornak, A. Hirshfeld, M. Ziliox, N. Syrett, P.J. Reeves, H.G. Khorana, M. Sheves, and S.O. Smith. 2009. Location of the retinal chromophore in the activated state of rhodopsin. J. Biol. Chem. 284: 10190–10201.

23. Lau, P.-W., A. Grossfield, S.E. Feller, M.C. Pitman, and M.F. Brown. 2007. Dynamic Structure of Retinylidene Ligand of Rhodopsin Probed by Molecular Simulations. J. Mol. Biol. 372: 906–917.

24. Jastrzebska, B., K. Palczewski, and M. Golczak. 2011. Role of bulk water in hydrolysis of the rhodopsin chromophore. J. Biol. Chem. 286: 18930–18937.

25. Leioatts, N., B. Mertz, K. Martínez-Mayorga, T.D. Romo, M.C. Pitman, S.E. Feller, A. Grossfield, and M.F. Brown. 2014. Retinal ligand mobility explains internal hydration and reconciles active rhodopsin structures. Biochemistry 53: 376–385.

26. Angel, T.E., S. Gupta, B. Jastrzebska, K. Palczewski, and M.R. Chance. 2009. Structural waters define a functional channel mediating activation of the GPCR, rhodopsin. Proc. Natl. Acad. Sci. U. S. A. 106: 14367–14372.

27. Altenbach, C., A.K. Kusnetzow, O.P. Ernst, K.P. Hofmann, and W.L. Hubbell. 2008. High-resolution distance mapping in rhodopsin reveals the pattern of helix movement due to activation. Proc. Natl. Acad. Sci. U. S. A. 105: 7439–44.

28. Mitchell, D.C., and B.J. Litman. 1999. Effect of Protein Hydration on Receptor Conformation: Decreased Levels of Bound Water Promote Metarhodopsin II Formation. Biochemistry 38: 7617–7623.

29. Mitchell, D.C., and B.J. Litman. 2000. Effect of Ethanol and Osmotic Stress on Receptor Conformation. Reduced Water Activity Amplifies the Effect of Ethnol on Metarhodopsin II Formation. J. Biol. Chem. 275: 5355–5360.

30. Dror, R.O., D.H. Arlow, P. Maragakis, T.J. Mildorf, A.C. Pan, H. Xu, D.W. Borhani, and D.E. Shaw. 2011. Activation mechanism of the β 2-adrenergic receptor. Proc. Natl. Acad. Sci. U. S. A. 108: 18684–18689.

31. Klauda, J.B., R.M. Venable, J.A. Freites, J.W. O'Connor, D.J. Tobias, C. Mondragon-Ramirez, I. Vorobyov, A.D. MacKerell, and R.W. Pastor. 2010. Update of the CHARMM All-Atom Additive Force Field for Lipids: Validation on Six Lipid Types. J. Phys. Chem. B. 114: 7830–7843.

32. Gawrisch, K., V.A. Parsegian, D.A. Hajduk, M.W. Tate, S.M. Gruner, N.L. Fuller, and R.P. Rand. 1992. Energetics of a hexagonal-lamellar-hexagonal-phase transition sequence in dioleoylphosphatidylethanolamine membranes. Biochemistry 31: 2856–2864.

33. Deupi, X., and J. Standfuss. 2011. Structural insights into agonist-induced activation of G-protein-coupled receptors. Curr. Opin. Struct. Biol. 21: 541–551.